Design issues and performance of a chemically recuperated aeroderivative gas turbine

C Carcasci[1], **B Facchini**[1] and **S Harvey**[2]
[1] Dipartimento di Energetica, University of Florence, Italy
[2] Department of Heat and Power Technology, Chalmers University of Technology, Göteborg, Sweden

Abstract: A number of innovative gas turbine cycles have been proposed lately, including the humid air turbine (HAT) and the chemically recuperated gas turbine (CRGT). The potential of the CRGT cycle lies in the ability to generate power with a high efficiency and ultra-low NO_x emissions. Much of the research work published on the CRGT cycle is restricted to an analysis of the thermodynamic potential of the cycle. However, little work has been devoted to discussion of some of the relevant design and operation issues of such cycles. In this paper, part-load performance characteristics are presented for a CRGT cycle based on an aeroderivative gas turbine engine adapted for chemical recuperation. The paper also includes discussion of some of the design issues for the methane–steam reformer component of the cycle. The results of this study show that large heat exchange surface areas and catalyst volumes are necessary to ensure sufficient methane conversion in the methane steam reformer section of the cycle. The paper also shows that a chemically recuperated aeroderivative gas turbine has similar part-load performance characteristics compared with the corresponding steam-injected gas turbine (STIG) cycle.

Keywords: chemical recuperation, methane–steam reforming, CRGT cycles, innovative gas turbine cycles, gas turbine cycle part-load performance simulation

NOTATION

d	diameter (m)
E_a	catalyst activation energy (J/mol)
F	mole flux (kmol/m^2_{cat} s)
H	heat exchanger height (m)
k	catalyst frequency factor (kmol/m^3_{cat} s bar)
L	heat exchanger length (m)
$\dot{m}$	mass flowrate (kg/s)
N_p	number of cold-side passes
N_r	number of tube rows per pass
P	power output (MW)
p_L	longitudinal tube pitch (m)
p_T	transverse tube pitch (m)
p	pressure (Pa)
p_{ref}	reference pressure = 101 325 Pa
$\dot{r}$	reaction rate (kmol/m^3_{cat} s)
R	universal gas constant = 8314.3 J/kmol K
T	temperature (K)
V	volume (m^3)
W	heat exchanger width (m)
X	mole fraction
z	reactor length spatial coordinate (m)
ΔT	temperature difference (K)
η	electric efficiency

Subscripts and superscripts

app	approach
cat	catalyst bed
cd	compressor discharge
cold	cold side
eq	equilibrium
exh	gas turbine exhaust
hot	hot side
Nom	nominal
PP	pinch point
s	steam

Abbreviations

CRGT	chemically recuperated gas turbine
FFC	fuel flow control
HRSG	heat recovery steam generator
IGV	inlet guide vane
MSR	methane–steam reformer
STIG	steam-injected gas turbine
SFC	steam flow control
TIT	turbine inlet temperature

The MS was received on 14 July 1998 and was accepted for publication on 9 September 1998.

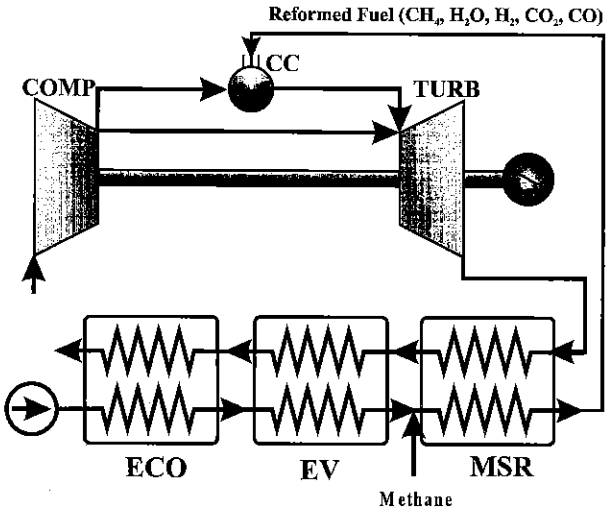

Fig. 1 CRGT cycle scheme applied to a two-shaft gas turbine: COMP, compressor; CC, combustion chamber; TURB, turbine; ECO, economizer; EV, evaporator

1 INTRODUCTION

The exhaust temperature of a gas turbine is usually between 700 and 900 K. The exhaust heat can thereafter be used to raise steam in a heat recovery steam generator (HRSG). The steam can be used either to provide heat or for additional power production by expansion in a steam turbine (combined cycle) or by re-injection into the gas turbine [steam-injected gas turbine (STIG) cycle]. To increase exhaust heat recovery further, the heat can be used to drive an endothermic chemical reaction resulting in the chemically recuperated gas turbine (CRGT) concept, originally proposed by Olmsted and Grimes [1]. In such a cycle (see Fig. 1), the superheater section of the HRSG is partially or totally replaced by a methane–steam reformer (MSR). Steam is raised in the low-temperature section of the HRSG and then mixed with natural gas before being fed into the MSR. In the reformer, the mixture is heated by the turbine exhaust, and an endothermic reaction occurs. The reformed fuel is then fed into the turbine combustor. Thus, the methane–steam mixture absorbs heat thermally (as the temperature increases), and chemically (as the endothermic reaction proceeds), resulting in a larger potential recuperation of exhaust energy than can be obtained by conventional recuperation. The cycle is very similar to an STIG cycle, with additional heat recovery by chemical recuperation. The thermodynamic advantage of the CRGT cycle over the STIG cycle can be understood by examining Fig. 2, which shows the temperature profiles in the heat recovery section of a CRGT cycle and the corresponding profiles for an STIG cycle. It is important to note that the comparison is made on the basis of identical steam flowrates in both cycles. This is because the amount of steam that can be injected into such cycles is strictly limited by the amount of extra flow that the turbine section of the cycle can accommodate, compared with the design value. The turbine exhaust conditions (flowrate and temperature) are also equal for both cycles if the turbine inlet temperatures (TITs) are taken to be equal. Figure 2 first shows the temperature profile of the hot turbine exhaust stream as it cools while providing heat to the steam or methane–steam mixture. The figure then shows the cold-side temperature profile for the STIG cycle. In the STIG cycle, water is pre-heated in an economizer, vaporized and superheated. As discussed above, the flowrate is limited by flow conditions in the turbine, and thus the limiting factor is the acceptable

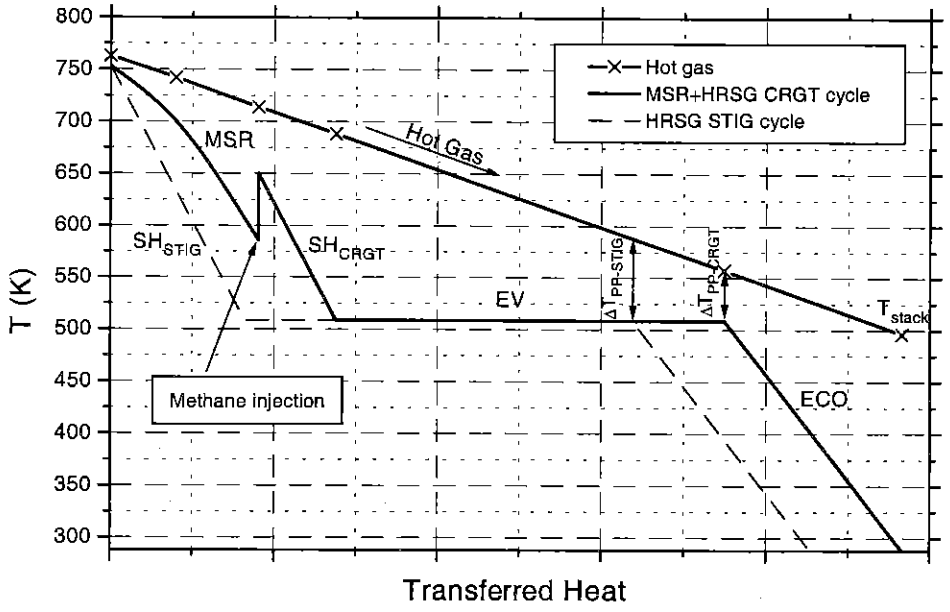

Fig. 2 Heat recovery temperature profiles for STIG and CRGT cycles

hot-end approach temperature difference. The CRGT cold-side temperature profile is now examined. From right to left, the temperature profiles in the economizer, evaporator and superheater sections are observed. Then the temperature drops as methane is injected into the main steam flow. The methane–steam mix then enters the catalytic reformer section, where the endothermic reforming reaction occurs. The effects of the endothermic reaction on the temperature profile can be seen clearly. The CRGT and STIG cycle profiles are now compared, recalling that the same steam flow is assumed, together with the same hot-end temperature approach. Given the endothermic nature of the reforming reaction, it can be seen that considerably more heat is exchanged in the MSR and CRGT superheater sections than in the STIG superheater section, for identical inlet and outlet temperatures. The temperature profiles in the economizer and evaporator are obviously identical. The net result is increased heat recovery, at the expense of a reduced pinch point temperature difference for the CRGT cycle, which thus requires a larger heat exchanger surface area. In terms of efficiency, the reformed fuel stream of the CRGT cycle has a higher potential heat content than the combined potential heat content of the superheated steam and fuel in the STIG cycle. Less fuel is therefore required to achieve the same TIT in the CRGT cycle, resulting in a higher efficiency.

1.1 Previous work and goal of present work

The CRGT cycle has received relatively little attention compared with other innovative gas turbine cycles. The CRGT cycle was considered by the collaborative advanced gas turbine (CAGT) program [2]. This program was initiated to promote research and development programmes for development of high-performance gas turbine cycles for intermediate and base load applications, using state-of-the-art aeroderivative gas turbine technologies. However, in the screening phases of the CAGT program, only a few of the possible CRGT cycle configurations were considered. Furthermore, no results were presented for part-load performance, which is an important comparison criterion for intermediate load cycles. Along the same lines, Lloyd [3] presented a detailed study of the thermodynamics of a number of CRGT cycles. However, the study did not contain any discussion of the part-load operating characteristics of the cycles considered. A discussion of some of the design issues of the MSR component of a CRGT cycle was presented by Adelman *et al.* [4]. The reactor geometry considered was a conventional tube-and-shell type of heat exchanger. However, as suggested by a number of researchers investigating the CRGT cycle (see, for example, references [5] and [6]), a more realistic design would be close to that of a standard HRSG, in which a catalytic steam reformer section would be added upstream of the superheater section. In such a design, the MSR reactor would be fully integrated with the steam generator in a single heat recovery device. In this paper, this reactor configuration is considered, and the sensitivity of the reactor design to variations in the key design parameters is analysed. The effects of these parameters on the performance of the overall cycle are also discussed.

Part-load performance is an essential comparison criterion for the intermediate-load power generation cycles. Very few studies have been published in the field of part-load CRGT cycle performance. A recent study was published by Botros *et al.* [7] discussing performance of a CRGT cycle used for mechanical drive application in pipeline compressor stations. The study included some results of part-load performance calculations for an RB211 aeroderivative engine. However, these workers assumed that the nominal and part-load performances of the simple cycle RB211 were unaffected by the cycle modifications implemented for CRGT operation. In this paper, performance predictions for part-load performance of a CRGT cycle based on the LM2500 aeroderivative gas turbine are presented. The simulation tools used allow the effects of cycle modifications on engine operation to be taken into account.

1.2 Cycle simulation tools

Given the complexity of CRGT plants, the proposed studies require the use of adequate plant performance simulation tools, with particular emphasis placed on part-load operation simulation capability. This work was performed using the modular code developed by Carcasci and Facchini [8]. The reader is referred to previous references [8], [9] and [10] for a complete presentation of the simulation tool used. A brief summary of the main features and assumptions is provided hereafter.

The most important feature of the modular simulation code developed by the present authors is the ability to simulate a new power plant configuration without creating a new source program. The code easily allows addition of new components. For this study, modules for design and off-design simulations of the MSR component were added. The power plant configuration is defined by connecting a number of elementary components representing different unit operations such as compressors, pumps, combustion chambers, splitters and mixers. Each component is defined as a black box capable of simulating a given chemical and thermodynamic transformation. The resulting set of non-linear equations defining the power plant is then linearized (the coefficients are, however, updated in the course of the calculation). All equations are then solved simultaneously using a classic matrix method; thus the procedure is essentially that of the fully implicit linear approach. Design and off-design simulation is a two-step procedure. Off-design performance simulation requires a geometric description of the different components (e.g. the velocity triangle at mean radius and other cascade parameters for the compressor or turbine, heat exchanger surface areas, etc.). These data result from a design study. When identifying the different parameters describing the component geometry, knowledge of some plant data is important to improve simulation results (e.g. the turbine exhaust flowrate and the temperature).

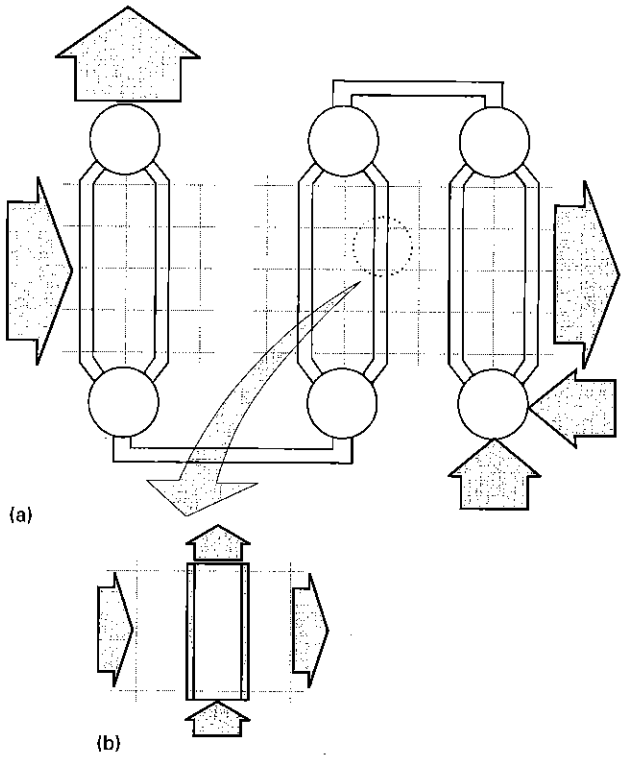

Fig. 3 (a) MSR reactor layout and (b) control volume

Off-design simulations are based on fixed geometry (obtained in the course of the design study), and there is thus a reduction in the number of input data.

2 MSR SIMULATION AND DESIGN ISSUES

In the present study, the MSR reactor configuration is similar to that of a traditional HRSG heat exchanger, with counter-cross flow of the hot and cold streams, as illustrated in Fig. 3. The hot turbine exhaust stream flows in the horizontal direction. The tubes contain catalyst pellets to enable the steam reforming reactions to occur. The tubes are positioned vertically, to prevent settling of the catalyst particles. Multiple rows of tubes per cold-side pass are considered, with perfect mixing assumed at the end of each pass. The model allows for finned or unfinned tubes. The user can specify transverse and longitudinal tube pitch and choose staggered or aligned reformer tubes.

The MSR is modelled by dividing it into control volumes (Fig. 3b). The equations used in a control volume of the MSR are mass, energy and chemical species balances. Finally, the hot gas flow is treated as a number of independent parallel layers, and lateral mixing is neglected. The equations used are now discussed in further detail.

2.1 Steam reforming chemistry

Within the MSR reaction zone, methane and steam react according to the following reactions [**11**]:

Table 1 MSR reaction kinetic constants

Reaction	k (kmol/m$^3_{cat}$ s bar)	E_a (J/mol)
1	24.54	53 131
2	1.64	26 794

$$CH_4 + 2H_2O \leftrightarrow CO_2 + 4H_2 \quad (1)$$

$$CO + H_2O \leftrightarrow CO_2 + H_2 \quad (2)$$

Given the high steam–carbon ratios considered, there is no risk of carbon coking [**11**]. Thus, reactions (1) and (2) are sufficient to describe the evolving composition of the reacting gas mix. The reformed gas mixture at the reformer exit contains a mixture of unconverted methane, H_2, CO_2, CO and large amounts of steam. Under the usual operating conditions, methane conversion is relatively low. Also, the shift reaction (2) usually results in low fractions of CO in the gas stream. As far as reaction rates are concerned, reaction (1) is kinetically controlled, whereas reaction (2) generally proceeds fast enough to be considered at equilibrium for the conditions considered. In this study, however, reaction kinetics for both reactions are considered. The reaction rates for reactions (1) and (2) are given by the following expressions [**12**]:

$$\dot{r}_1 = -\frac{dF_{CH_4}}{dz} = k_1 \exp\left(\frac{-E_{a1}}{RT}\right) \frac{p_{CH_4} - p_{CH_4,eq}}{(p_{H_2O}/p_{ref})^{0.596}} \quad (3)$$

$$\dot{r}_2 = -\frac{dF_{CO}}{dz} = k_2 \exp\left(\frac{-E_{a2}}{RT}\right) (p_{CO} - p_{CO,eq}) \quad (4)$$

with F_{CH_4} and F_{CO} denoting the mole fluxes of CH_4 and CO respectively. The catalyst frequency factors k and activation energies E_a for the two reactions are given in Table 1. The catalyst is a conventional alumina-supported nickel catalyst in cylindrical pellet form. $p_{CH_4,eq}$ and $p_{CO,eq}$ in equations (3) and (4) respectively denote the partial pressures of CH_4 and CO at equilibrium.

Using the reaction rates, the mole flowrate variations of each species in the catalyst bed control volume can be determined.

2.2 Heat transfer and pressure drop

Inside the reformer tubes, the catalyst bed has a strong effect on the local heat transfer and pressure drop coefficients. An empirical correlation for a cylindrical-particle packed bed from Li and Finlayson [**13**] was used in the present study. The total pressure drop is calculated for each control volume using the Ergun equation [**14**] for frictional pressure drop through a fixed particle bed. For the hot-side heat transfer coefficient and pressure drop calculations, standard correlations for HRSG calculations are used from Vampola [**15**].

2.3 MSR geometry considerations

Design of the MSR heat recovery device involves a somewhat complex trade-off. The geometry selected should not only favour heat exchange but also allow a sufficient residence time of the reforming gas in the MSR, so that the endothermic reaction can come close to chemical equilibrium. Furthermore, hot-side and cold-side pressure drops should be as low as possible: the former to decrease the gas turbine back pressure, and the latter to favour methane conversion (methane conversion at equilibrium is favoured by low pressure). Finally the dimensions of the MSR section of the heat recovery device should be reasonable compared with those of the steam generator and the gas turbine.

The aim of this paper is to discuss the main design issues for the MSR component. Thus, it is important to identify the parameters that influence MSR performance (i.e. methane conversion). Methane conversion depends on residence time, which is essentially proportional to catalytic reactor bed volume; this can be expressed as follows:

$$V_{\text{cat}} = \frac{\pi}{4} \frac{WLH}{(p_{\text{T}}/d_{\text{i}})(p_{\text{L}}/d_{\text{i}})} \tag{5}$$

Thus, if the aim of the design is to maximize methane conversion, the following may be concluded:

1. The transverse tube pitch and the longitudinal row pitch should be as small as possible without resulting in an excessive hot-side pressure drop. In this study the tube and row pitches are therefore fixed at 1.5, which corresponds to the lowest value adopted in standard HRSG design practice (see reference **[16]**).
2. The MSR width and height should be as large as possible, resulting in a low cold-side pressure drop and an acceptable MSR length. The MSR width is therefore fixed at 6.0 m (i.e. slightly wider than the LM2500 gas turbine selected for this study), retaining the MSR height as the only dimensional variable.

The design variables retained for the analysis are thus the tube diameter, the number of tube rows per cold-side pass, the number of cold-side passes and the MSR height. It should also be noted that the fin geometry has little effect on the results since heat exchange is not a problem for the cases considered (the hot-end approach is low in all cases). Thus, the effects of fin geometry will not be discussed further in this paper.

2.4 MSR design issues: results and discussion

A CRGT cycle has similar flow characteristics to an STIG cycle. In this study, computed performance characteristics are presented for the MSR component of a CRGT cycle based on General Electric's LM2500 aeroderivative STIG. Table 2 shows the main operating characteristics of this gas turbine. Table 3 shows the geometry data retained for the MSR component of the CRGT cycle. The MSR hot-side inlet flow conditions are set equal to those of the gas turbine exhaust. The steam flowrate is set equal to that of full steam injection in the LM2500 STIG machine (i.e. 50 000 lb/h). The steam is superheated to 650 K before entering the MSR, since catalytic activity is very low below this temperature. It should be noted that it is thereby assumed that the reformed gas stream entering the combustion chamber in the CRGT cycle can be hotter than the design temperature of the steam injected into the STIG cycle. The steam–methane ratio is the same as used in reference [4]. The LM2500 is approximately 4.2 m in width and 4.4 m in height. As discussed previously, the MSR width and maximum allowable height are fixed at 6.0 m. The other geometric parameters (see Table 3) are fixed according to standard HRSG design practice.

A reactor catalyst bed volume of 40 m^3 was selected as a reference value, based on results obtained by Adelman *et al.* [4] which indicate that this volume is necessary for satisfactory methane conversion under the reactor operating conditions considered.

Figure 4 shows the hot-end temperature approach ΔT_{app} as a function of catalyst volume V_{cat} for two different heat

Table 2 LM2500 and LM2500 STIG performance characteristics

	LM2500 PE*		LM2500 PH STIG†	
Characteristic (units)	General Electric	Code	General Electric	Code
Output power‡ (kW_e)	22 800	22 800	27 400	27 400
Electrical efficiency	0.3754	0.3752	0.4130	0.4146
Shaft speed (Hz)	60	60	60	60
Exhaust flow (kg/s)	68.95	68.95	75.3	75.3
Exhaust temperature (K)	796.5	796.5	773.2	764.2
Pressure ratio	18.8	18.8	20.2	20.1
Steam flowrate (kg/s)	—	—	6.3	6.3
Steam temperature (K)	—	—	588.7	588.7
HRSG surface area (m^2)	—	—	Not applicable	3458
Steam pressure (kPa)	—	—	2757.9	2757.9

* Rating: at 15 °C; sea level; no inlet or exhaust losses and natural gas.
† Rating: at 15 °C; sea level; 4 in/10 in inlet/exhaust losses and natural gas.
‡ At generator terminals.

Table 3 MSR geometry data

Hot-side flowrate (kg/s)	76.2
Hot-side inlet temperature (K)	770
Hot-side inlet pressure (Pa)	104 000
Steam flowrate (kg/s)	6.3
Steam–methane molar ratio	6.194
Steam inlet temperature (K)	650
Steam inlet pressure (MPa)	3.64
Width W (m)	6
Height H (m)	4.0–6.0
Tube outer diameter (d_{tube}) (mm)	50.8–101.6
Transverse tube pitch p_T/d_{tube}	1.5
Longitudinal row pitch p_L/d_{tube}	1.5
Tube arrangement	Staggered
Fin thickness (% of d_{tube})	2.0
Fin height (% of d_{tube})	20.0
Fin spacing (% of d_{tube})	20.0
Number of passes N_p	6–16
Number of rows per pass N_r	2–4

exchanger heights H (i.e. 4.0 and 6.0 m) and various numbers of tube rows N_r per cold-side pass (i.e. 2, 3 and 4). As expected, the hot-end temperature approach decreases as the catalyst volume is increased (i.e. as the heat exchanger surface area is increased). However, it is important to realize that ΔT_{app} is low (i.e. less than 5 K) for all cases considered. This is an important aspect of MSR design for CRGT cycles; sufficient heat exchange and low hot-end temperature approaches are usually achieved more easily than sufficient methane conversion and reasonable pressure drops.

Figure 5 shows that methane conversion increases as the catalyst bed volume is increased since the gas residence time increases. Methane conversion is defined as the difference between the methane mole fraction at the reactor input and that at the output, referred to the input mole fraction:

$$\text{Methane conversion} = 1 - \frac{X_{CH_4,out}}{X_{CH_4,in}} \tag{6}$$

The figure also shows that the heat exchanger height has little influence on methane conversion. For a given catalyst volume, the results seem to suggest that a small number of tube rows per pass results in improved methane conversion. However, methane conversion is best evaluated by comparison with the corresponding chemical equilibrium conditions, i.e. by the ratio $(X_{CH_4,out,eq} - X_{CH_4,out})/X_{CH_4,in}$ as shown in Fig. 6. In Fig. 6, the difference between the reactor outlet methane composition at equilibrium and that under real conditions is computed. This difference is then related to the inlet methane composition. The figure shows that many tube rows per pass in fact lead to an exit composition closer to equilibrium. A significant improvement in methane conversion relative to equilibrium can be observed when the number of tube rows per pass is increased from two to three. The improvement is much less pronounced when the number is further increased from three to four. The explanation for the difference between Figs 5 and 6 is the cold-side pressure drop (Fig. 7), which influences the reference equilibrium composition [the equilibrium of reaction (1) is highly sensitive to pressure]. It is important to note that the results presented in this section consider a fixed MSR cold-side inlet pressure (computationally less cumbersome). Several runs were also performed with fixed cold-side outlet pressure (corresponding to real MSR operating conditions), and the results obtained were very similar. Figure 7 shows that, with few tube rows N_r per pass, the reforming gas pressure drop is higher than that with many tube rows per pass

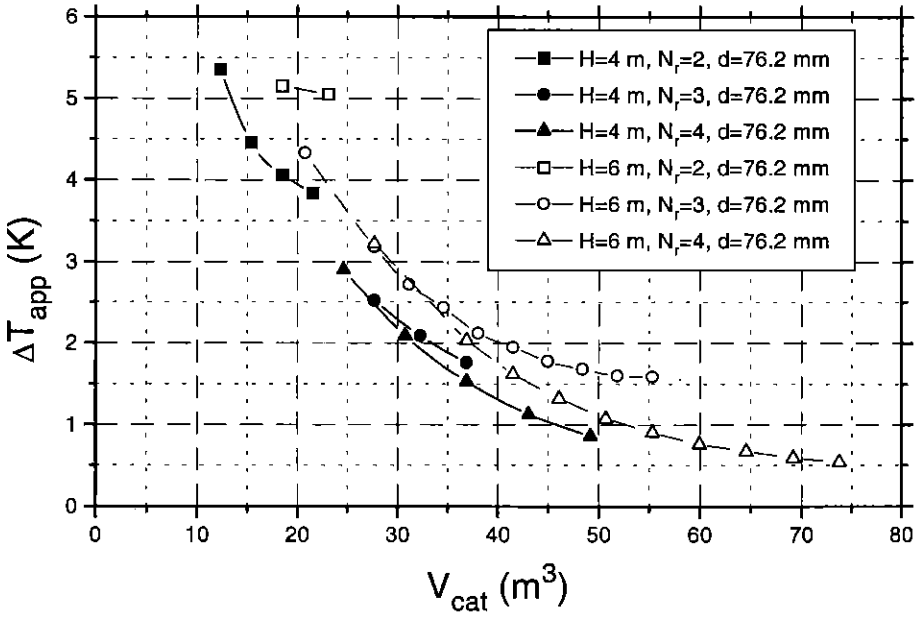

Fig. 4 Hot-end temperature approach versus catalyst volume (fixed tube diameter)

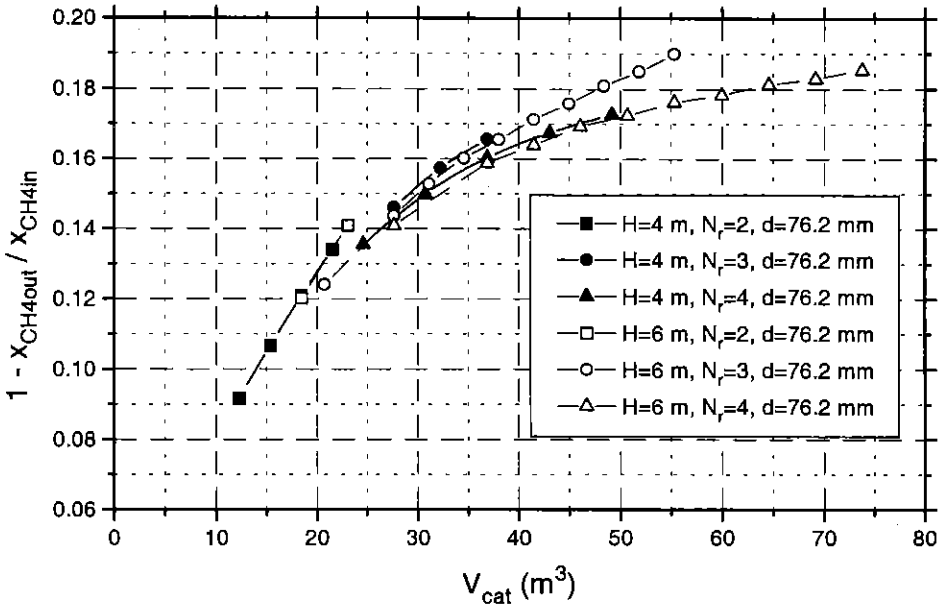

Fig. 5 Methane conversion versus catalyst volume (fixed tube diameter)

because the reforming gas velocity increases. The figure also shows that heat exchanger height does not influence the reforming gas pressure drop. Figure 8 shows that the hot gas pressure drop increases with increasing catalyst volume because the total number of tube rows increases. The hot-side pressure drop increases as the heat exchanger height decreases because the hot gas velocity increases. Thus, an MSR should in theory be as high as possible. In this study, the MSR height is limited to 6.0 m (i.e. a reasonable size compared with the gas turbine, as discussed previously).

All results shown in this section were obtained assuming a fixed reformer tube diameter. The effects of varying this diameter were also analysed, and it was concluded that the tube diameter should be large. In this study the tube diameter was limited to 76.2 mm (3 in).

At this point of the study, the following may be concluded:

1. The heat exchanger height should be as large as possible (limited to 6.0 m in this study).
2. The tube diameter should be large (limited to 76.2 mm).

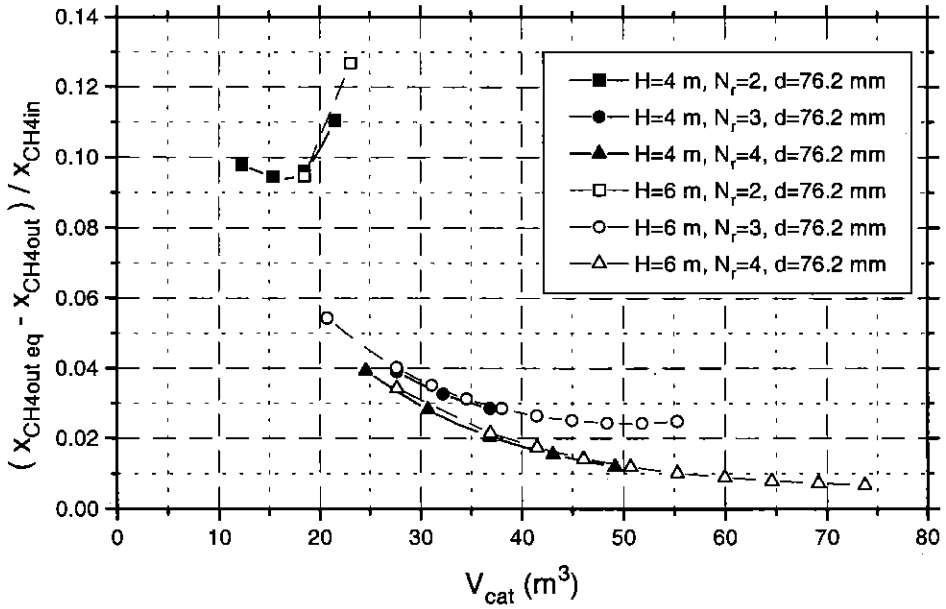

Fig. 6 Methane conversion relative to equilibrium versus catalyst volume (fixed tube diameter)

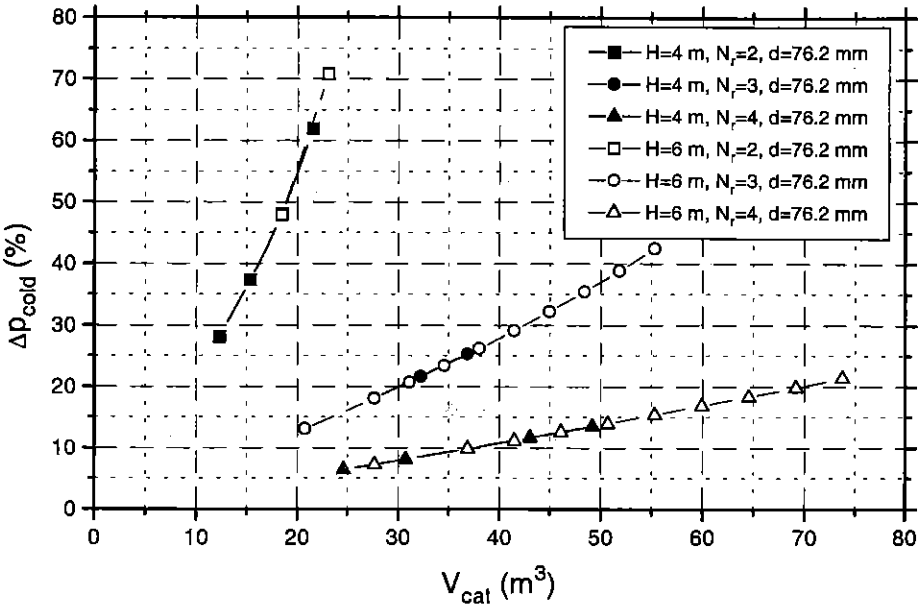

Fig. 7 MSR cold-side pressure drop versus catalyst volume (fixed tube diameter)

3. The number of tube rows per pass should be large, but incremental improvements are small beyond three tube rows per pass (a limit of four tube rows per pass was considered).

The optimal catalyst volume should be selected on the basis of good methane conversion with acceptable hot-side and cold-side pressure drops. However, identification of the optimal catalyst volume depends primarily on catalyst costs and requires a thermoeconomic analysis of the cycle, which is beyond the scope of this study.

Based on the results obtained, several MSR configurations appear to be of interest: eight passes with three or four tube rows per pass, and ten passes with three tube rows per pass. Table 4 summarizes the main characteristics of these configurations. In order to proceed with the next part of this study (i.e. simulation of full-load and part-load operation of an LM2500 aeroderivative gas turbine adapted for CRGT operation), it is necessary to select an MSR configuration. For this purpose, the configuration with eight cold-side passes and three tube rows per pass was retained. This configuration results in lower methane conversion, but

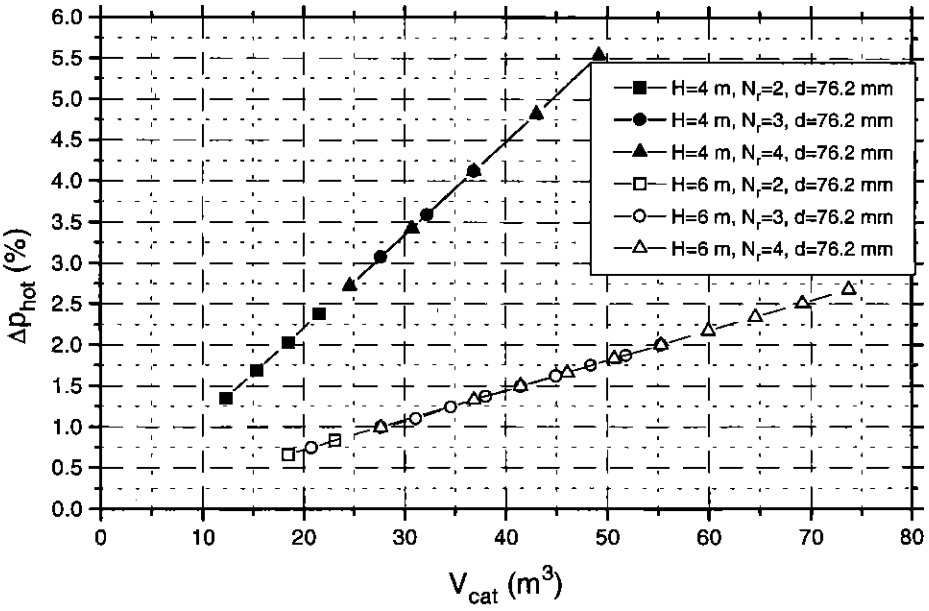

Fig. 8 MSR hot-side pressure drop versus catalyst volume (fixed tube diameter)

Table 4 Summary of various MSR reactor characteristics

	Dimensions $W \times H \times L$ (m × m × m)	N_p	N_r	d_{tube} (mm)	ΔT_{app} (K)	$1 - X_{CH_4,out}/X_{CH_4,in}$	$(X_{CH_4,out,eq} - X_{CH_4,out})/X_{CH_4,in}$	Δp_{hot} (%)	Δp_{cold} (%)
Case 1	6×6×2.74	8	3	76.2	3.15	0.1430	0.1823	0.99	17.60
Case 2	6×6×3.66	8	4	76.2	2.16	0.1612	0.1851	1.33	11.25
Case 3	6×6×3.43	10	3	76.2	2.27	0.1557	0.1839	1.25	20.81

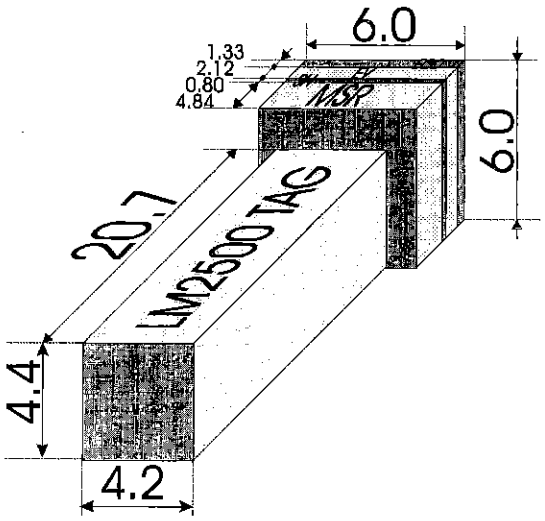

Fig. 9 Estimated dimensions (in metres) of LM2500 CRGT

with a low hot-side pressure drop. Compared with other possible configurations considered, this leads to a relatively small catalyst volume (and thus low capital costs) with only a small corresponding decrease of power output and efficiency. Figure 9 gives an idea of the main dimensions of the plant, showing how the MSR component is larger than the steam generator component (4.84 m compared with 4.25 m).

Before concluding this first part of the study, it is also interesting to examine cold-side temperature profiles (Fig. 10) and reforming reaction rate profiles (Fig. 11) within the MSR (the figure shows results for a reactor with eight cold-side passes and four tube rows per pass). For each pass there are four profiles corresponding to the four tube rows per pass. The figure illustrates the mixing process occurring between successive cold-side passes. The reforming gas temperature increases rapidly in the first cold-side pass, since the temperature difference between the hot-side and the cold-side streams is large. The rate of increase is reduced in the subsequent passes because the temperature difference decreases. The figure thus confirms that little heat transfer occurs in the final passes, and the main function of these passes is to allow sufficient residence time in the catalytic bed so that the steam reforming reaction can continue to proceed and approach equilibrium. Figure 11 shows the reaction rate $\dot{r}$ of reaction (1) in the MSR. In the first pass, $\dot{r}$ is initially low owing to the low reforming

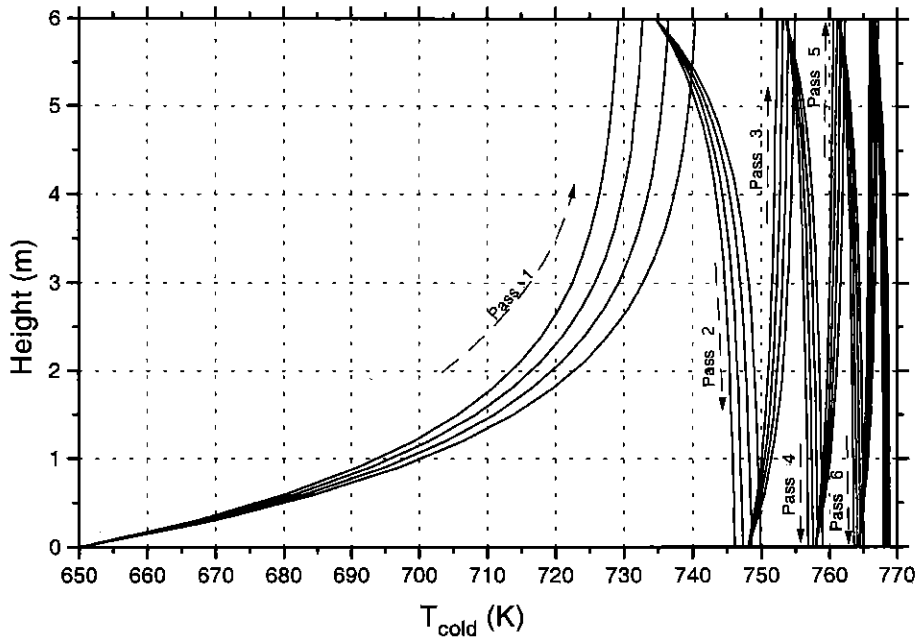

Fig. 10 MSR cold-side temperature profiles ($N_p = 8$; $N_r = 4$)

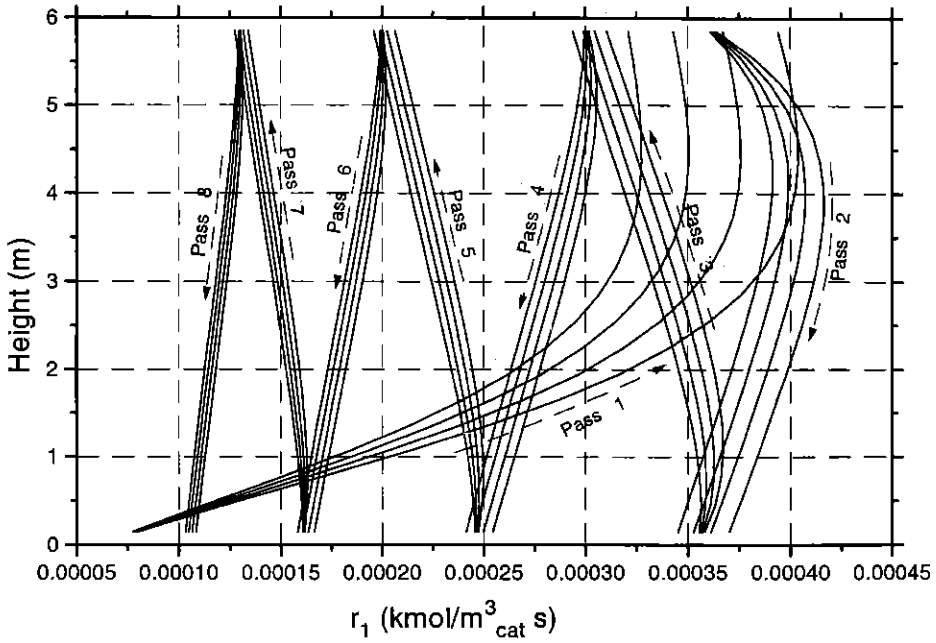

Fig. 11 MSR reforming reaction rate profiles ($N_p = 8$; $N_r = 4$)

gas temperature. However, the reaction rate increases rapidly as the temperature increases, and the reaction proceeds rapidly since the gas composition is initially far from equilibrium. The reaction rate decreases further through the reactor as the gas composition approaches equilibrium. At the MSR cold-side exit, the gas is relatively close to equilibrium. The important point to note about these two figures is that the rate of temperature increase in the final passes is very low, whereas the rate of reaction rate decrease is much less pronounced. This confirms that the final tube rows are necessary, not so much to attain a satisfactory hot-end temperature approach, but mostly to achieve a satisfactory degree of methane conversion.

2.5 MSR design issues: conclusions

In this first part of the paper, some of the design issues for the MSR component of a CRGT cycle have been discussed. The results show that design of this component is more complex than that of the superheater section of a heat recovery steam generator, since the MSR component must allow sufficient heat transfer while at the same time allowing sufficient residence time (i.e. methane conversion). The study shows that this leads to large heat exchanger surface areas and catalyst bed volumes. Further discussion of MSR design therefore requires a thermoeconomic analysis of the cycle, which is beyond the scope of this paper. The important issues are methane conversion and hot-side pressure drop. Increasing the catalyst bed volume improves methane conversion but also increases the hot-side pressure drop (detrimental to cycle performance) and obviously increases the size and cost of the MSR component of the cycle.

3 SIMULATION OF A CHEMICALLY RECUPERATED AERODERIVATIVE GAS TURBINE

A CRGT power plant has similar flow characteristics to an STIG plant. Thus, when selecting a gas turbine for such a plant, priority should be given to an engine that has already been adapted for STIG operation. Furthermore, as discussed in the introduction, chemically recuperated cycles appear particularly attractive for high-efficiency intermediate-load operation. This type of operation implies frequent start-ups and load variation. Based on these criteria, modern aeroderivative gas turbines seem well suited to CRGT operation. In this study, the performance of a CRGT cycle based on the commercially available LM2500 STIG engine is examined. The LM2500 industrial gas turbine is General Electric's most proven aeroderivative engine. It is derived from the TF-39 flight engine and many units are now in land and marine service. The engine is of the two-shaft type with a single-rotor gas generator unit followed by a separate power turbine. The compressor is a 16-stage axial flow design with inlet guide vanes (IGVs) and variable-area vanes on the first six stator stages. The combustion chamber is of the annular type. A two stage high-pressure turbine drives the compressor; both stages of nozzle and turbine blades are air cooled [**17**].

In the STIG cycle, steam is typically produced in an HRSG and is then injected into the gas turbine. The additional mass flow that can be expanded in the standard LM2500-PE gas turbine is limited. A modified version (LM2500 PH) has a slightly increased high-pressure turbine inlet area and slightly decreased power turbine inlet area; thus it is able to accommodate higher amounts of steam and to provide better performance in STIG operation [**17**].

Table 5 LM2500 CRGT characteristics ($N_p = 8$; $N_r = 3$)

Compressor air flowrate (kg/s)	67.96
Compression ratio	19.81
Turbine inlet temperature (K)	1446.2
Nominal load power output (MW_e)	28.00
Thermal efficiency	0.4576
Turbine exhaust flowrate (kg/s)	75.48
Turbine exhaust temperature (K)	762.4
Steam flowrate (kg/s)	6.298
HRSG pinch point ΔT (K)	48.4
HRSG heat exchange surface area (m^2)	6331
MSR heat exchange surface area (m^2)	6090
Methane conversion in MSR (%)	10.87
Reformed fuel composition (molar)	
CH_4	0.153 58
H_2O	0.753 49
H_2	0.074 20
CO_2	0.018 01
CO	0.000 72
MSR hot-end temperature approach (K)	4.09
Turbine exhaust pressure (kPa)	103.6
MSR hot-side pressure drop (%)	0.93
MSR cold-side pressure drop (%)	28.51
Methane–steam ratio (molar)	4.586
Catalyst volume (m^3)	27.66

Table 2 lists the manufacturer's published performance data for the PE and steam-injected PH engines, taken from reference [**18**]. Results generated using the present authors' cycle simulation code are also listed, showing good agreement at ISO operating conditions. Results were also generated for other ambient temperature values ranging from 255 to 310 K. Reasonably good agreement was found between the simulation results and the manufacturer's performance curves. The reader is referred to another paper by the present authors for a more detailed discussion of these results [**19**].

Table 5 shows results for simulated nominal load performance characteristics of the chemically recuperated cycle, based on the selected MSR configuration discussed previously in this paper. When comparing Tables 2 and 5 it is important to recall that the steam flowrates are the same for the STIG cycle and the CRGT cycle. The CRGT cycle has a similar power output (28.0 MW compared with 27.4 MW for the STIG cycle) which is normal given the similar mass flowrates through both engines. The efficiency is, however, much higher for the CRGT cycle (45.76 per cent versus 41.46 per cent for the STIG cycle), which demonstrates the effectiveness of the chemical recuperation concept, despite the low methane conversion (10.9 per cent) in the MSR reactor for the case considered. It is also important to recall that the temperature of the steam injected into the STIG cycle is 588.7 K, which results in a large temperature difference in the recovery boiler. For the CRGT cycle, it was assumed that the temperature difference could be decreased in order to allow increased heat recovery. It was also assumed that the reformed gas temperature (758.3 K) could be increased compared with the STIG cycle steam temperature, thereby favouring methane conversion in the MSR. This of course leads to substantially larger heat exchanger areas for the CRGT cycle, as shown in Tables 2 and 5.

3.1 Part-load operating strategies for STIG and CRGT cycles

First the STIG cycle case is discussed. It is assumed that the maximum temperature at which the steam can be re-injected into the gas turbine is fixed. If all steam produced in the HRSG is re-injected into the gas turbine, the two main quantities that can be varied in order to reduce the power output of the turbine are the maximum turbine inlet temperature (TIT) or one of the steam parameters, i.e. the pressure or the flowrate. Steam can also be used for cogeneration purposes, if a bleed valve is installed at the exit of the HRSG. In this case, another degree of freedom is added; therefore in this case three quantities can be varied (the TIT, p_s and $\dot{m}_s$). Other power control systems include variation of the compressor IGVs. It is important to emphasize that, at part load, the steam temperature is determined by the flow conditions through the HRSG and therefore cannot be varied independently.

Discarding the cogeneration case for the moment, if a constant steam flowrate $\dot{m}_s$ is imposed and the TIT is decreased, the steam pressure p_s becomes too small for re-injection into the gas turbine, and this power reduction system is thus not feasible. Therefore, the steam pressure must be fixed and the TIT must be used as the power control variable. The TIT is determined by the fuel flowrate; thus this power reduction system is called fuel flow control (FFC). Under these conditions, $\dot{m}_s$ is determined by the HRSG operating conditions and cannot be varied independently. The steam pressure must be low in order to obtain the best efficiency, because in this case the steam flowrate is highest. It is concluded that the steam–air pressure ratio p_s/p_{cd} in the combustion chamber should be set at the minimum allowable value (i.e. the steam pressure must be equal to the sum of the compressor discharge pressure plus all relevant pressure drops in the steam system).

The cogeneration case is now considered. Steam can be bled off at the HRSG outlet, and an additional degree of freedom is thus introduced. Maintaining the minimum steam–air pressure ratio p_s/p_{cd}, the steam flowrate $\dot{m}_s$ injected into the turbine is now independent of the TIT. Under full-load operating conditions, the HRSG pinch point temperature difference of the simple STIG cycle is very high. This enables a large amount of steam to be raised and used for cogeneration purposes, if the HRSG is oversized. At part load, a control system which maintains a constant steam flowrate injected into the gas turbine ($\dot{m}_s$ = constant) can be used. As the TIT is decreased, the overall steam flowrate of course decreases although the gas turbine steam injection flowrate is maintained constant, and the cogeneration steam flowrate is gradually reduced.

A second load reduction system is possible for cogeneration plants: steam flow control (SFC) (i.e. varying the steam mass flowrate injected into the turbine) coupled

with fixed turbine inlet temperature (for SFC, TIT = constant). This control system does not require oversizing the HRSG. In effect, at part load the steam flowrate generated in the evaporator decreases a little (owing to a decrease in the turbine exhaust flowrate), whereas the steam flowrate injected into the turbine decreases strongly. Thus, at part load, the steam flow available for cogeneration utility increases. This control system is convenient for cogeneration plants where the electric power load usually decreases while the heat load increases. However, for applications where the electricity load decreases simultaneously with the heat load, the other control system (for FFC, $\dot{m}_s$ = constant) is preferable.

For the CRGT cycle, addition of the MSR to the HRSG theoretically adds a further degree of freedom, namely the methane–steam ratio. However, in practice, there is very little degree of freedom for the methane–steam ratio when other operating constraints are accounted for. This is because the methane flowrate is essentially determined by the chosen value for the TIT, and the steam flowrate by either the HRSG operating conditions (if all the steam is re-injected into the gas turbine) or by the cogeneration steam flow setting. Thus, the methane–steam ratio cannot be varied independently, and the considerations discussed previously for load variation of STIG cycles are valid for CRGT cycles.

3.2 Part load of LM2500 CRGT and LM2500 STIG: simulation results

Figure 12 shows the relative power–efficiency curves referred to nominal ISO load values, for the STIG cycle and the CRGT cycle. The results for different load reduction control strategies are shown. The results for the dry cycle with FFC are also shown for reference. Figure 13 shows the corresponding variations in the turbine exhaust temperature.

First the case is considered where the HRSG is dimensioned for the nominal STIG steam injection flowrate (i.e. without provision for additional cogeneration steam). If a constant steam–air pressure ratio p_s/p_{cd} is maintained and the FFC scheme (for FFC, p_s/p_{cd} = constant) is used, the steam flowrate $\dot{m}_s$ and the turbine exhaust temperature both decrease as the TIT is decreased. In this case, the CRGT and the STIG performance are both better than the dry cycle performance.

The cogeneration case is now considered. Figure 12 shows that part-load operation with fixed steam injection flowrate (for FFC, $\dot{m}_s$ = constant; with oversized HRSG and progressive reduction in cogeneration steam flowrate) gives the best performance for the STIG and CRGT cycles. The efficiency trend of the CRGT cycle is worse than that of the STIG cycle because the decrease in the turbine exhaust temperature is more penalizing for the CRGT cycle (since methane conversion decreases with decreasing temperature of the reforming gas stream). When the cogeneration steam flow is reduced to zero further power reduction is not possible with this control system. The point at which this limit is reached depends on the minimum allowable pinch point temperature difference in the HRSG. This point is reached more rapidly for the CRGT cycle (Fig. 12), because the pinch point temperature difference at design conditions is already low, since more exhaust heat is recovered in the CRGT cycle than in the STIG cycle. Part-load operation

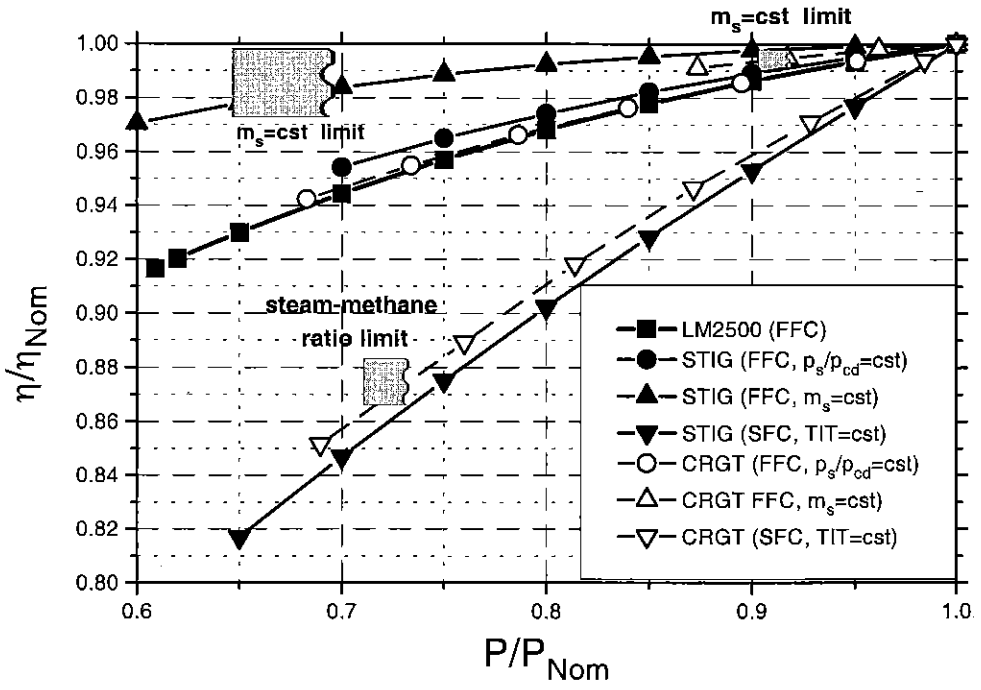

Fig. 12 Electrical efficiency versus power (cst = constant)

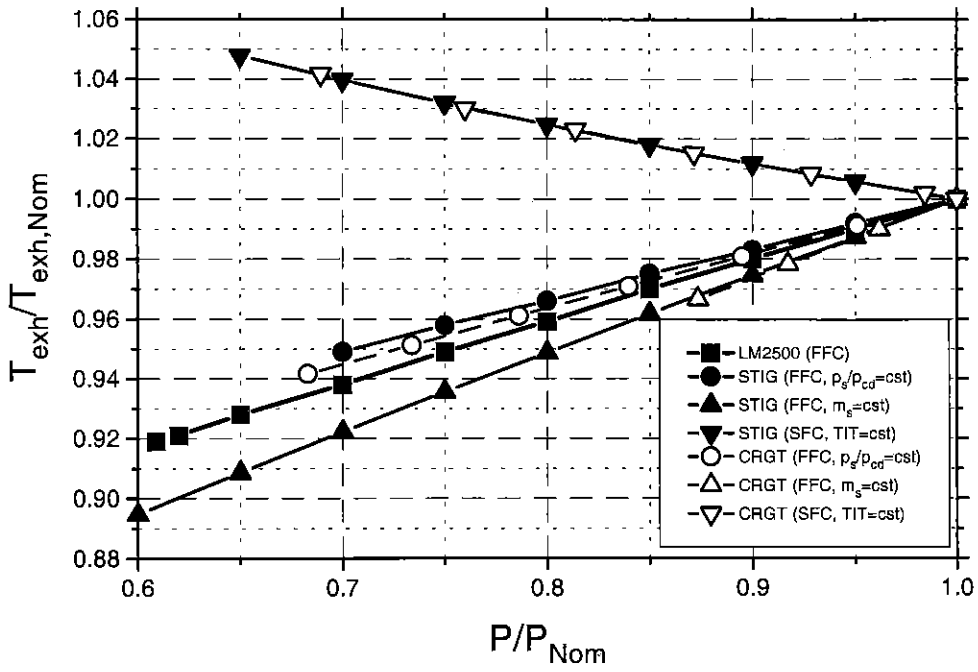

Fig. 13 Turbine exhaust temperature versus power

of the CRGT cycle is further limited by the increase in the molar steam–methane ratio which cannot exceed six for combustion stability purposes. However, the pinch point limit is usually reached before the steam–methane ratio limit.

The other cogeneration configuration is now considered. Power reduction is achieved by maintaining the TIT constant and decreasing the steam flowrate injected into the gas turbine (for SFC, TIT = constant; cogeneration steam produced without oversizing of the HRSG). In this case, the efficiency trend for both advanced cycles is worse than for the dry cycle. However, the efficiency trend is better for the CRGT cycle than for the STIG cycle since the exhaust temperature increases at part load (Fig. 13). Again, a further limitation exists for the CRGT cycle; the steam–methane ratio cannot drop below three as the steam flowrate is decreased. This avoids carbon formation in the MSR.

Comparing the trends of the SFC and MSR control systems, it is observed that decreasing the steam flowrate has a pronounced negative impact on efficiency for both the STIG and the CRGT cycles. It is concluded that the variations in efficiency of the CRGT cycle at part load compared with the STIG cycle are due mainly to the variations in steam flow and to a lesser extent to the variations in methane conversion in the MSR. It is important to note that, although the STIG efficiency trend at part load is equal to or better than that of the CRGT cycle, the absolute efficiency values are significantly better for the CRGT cycle. The reference nominal efficiencies and power outputs can be found in Tables 4 and 5. On the basis of these values, it should be noted that the CRGT cycle efficiency at 70 per cent of full load is higher than that of the STIG cycle at full load.

It is important to note that the turbine exhaust flowrate of all cycles decreases at part load owing to a reduction in the speed of the high-pressure shaft. This decrease is more pronounced for the STIG and CRGT cycles than for the dry cycle, particularly when the SFC system is used. The steam pressure decreases at part load for all control systems because the gas turbine compression ratio always decreases at part load. This fact, coupled with the fixed ratio of steam to air pressure, allows only a limited steam flow reduction.

The variation in the methane conversion efficiency of the CRGT cycle at part load is shown in Fig. 14. The observed decrease is due predominantly to the reduction in the turbine exhaust temperature (for the FFC configurations), although the steam–methane ratio increases slightly and the steam pressure decreases. When SFC is adopted, the steam–methane ratio decreases significantly, resulting in a larger methane conversion efficiency decrease.

Figure 15 shows the efficiency trend using the compressor IGV control system. This control method has a smaller power reduction scope (5–10 per cent of P_{Nom} for the gas turbine considered). However, it permits good part-load performance, particularly for the CRGT cycle, because of the positive effects of compression ratio reduction and increased turbine exhaust temperature. Both effects improve the methane conversion efficiency in the reforming process, resulting in superior performance for the CRGT cycle. The same effects improve the efficiency of the STIG cycle, but to a lesser extent.

To summarize the results of this section, the part-load performance characteristics of a CRGT cycle were presented and compared with those of the same aeroderivative gas turbine with and without steam injection. The improved performance of the injected cycles was confirmed and

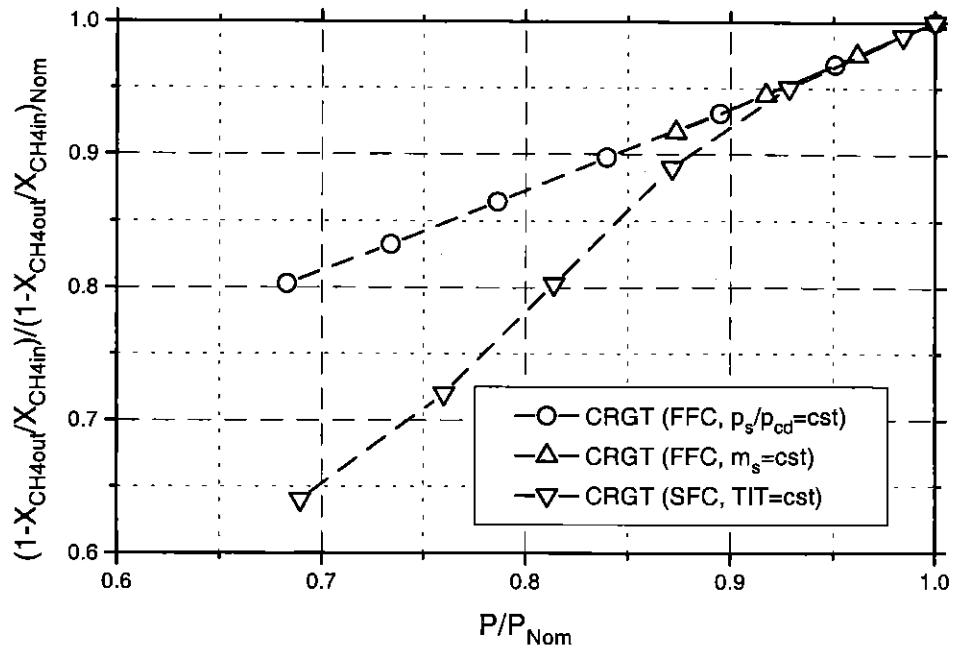

Fig. 14 Methane conversion versus power (LM2500 CRGT)

similar part-load behaviours of the STIG and CRGT cycles were observed. The variations in the turbine exit temperature and steam flow are the most important factors that affect part-load performance of the chemical recuperator component of the cycle.

4 CONCLUSIONS

Chemically recuperated cycles have the potential for high power generation efficiency and are similar in many ways to STIG cycles. In this work, a CRGT cycle based on the LM2500 aeroderivative STIG was studied. The results show CRGT nominal load efficiency values more than four percentage points above the efficiency values for the STIG cycle, confirming the thermodynamic benefit of the chemical heat recovery concept. Part-load behaviour of the CRGT cycle is very similar to that of the STIG cycle and depends essentially on the amount of steam injected into the cycle in both cases. The impact of decreased

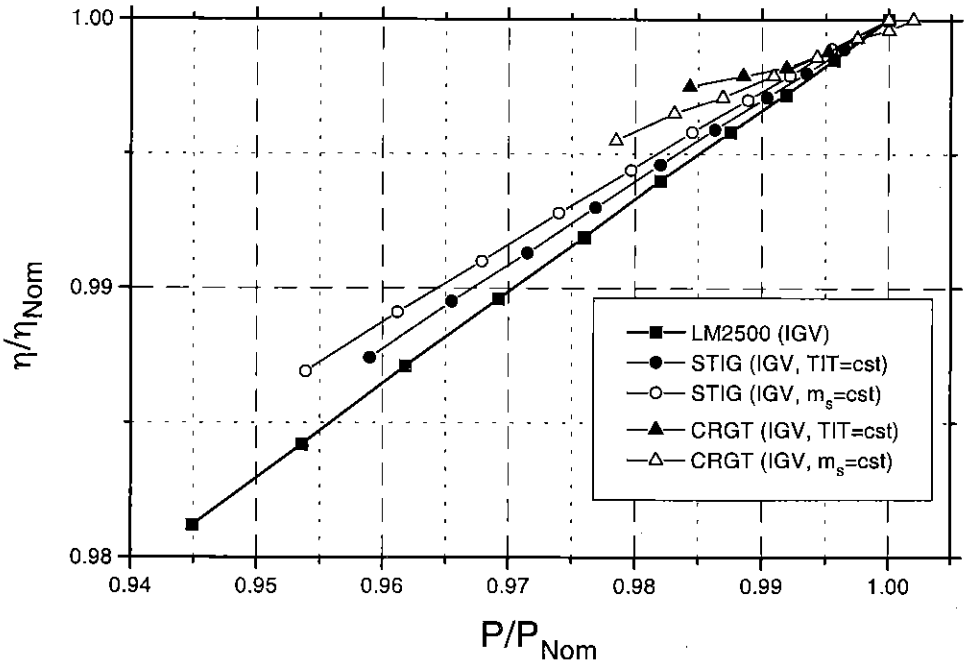

Fig. 15 Efficiency versus power using IGV power output control

methane conversion at part load on the efficiency of the CRGT cycle is shown to be minimal compared with the impact of decreased steam flow. The study also examined some of the important issues for design of the MSR component of the cycle. The chosen reactor configuration was that of a standard HRSG, with an additional high-temperature reformer reaction section upstream of the steam superheater. It was shown how large heat exchanger surface areas are needed to allow the methane–steam reforming reactions to approach equilibrium conversion, thus maximizing chemical heat recovery in the cycle.

The conclusions of this study are that, in comparison with the corresponding STIG cycle, a CRGT cycle requires a considerably larger heat exchange area, and a large volume of expensive catalyst. To reduce these requirements, catalysts specially developed for the CRGT cycle must be found, with high activities at relatively low temperature levels. In terms of performance, the CRGT cycle has an improved efficiency over the STIG for a similar power output. The part-load operating characteristics are much the same for both cycles, with added constraints for the CRGT cycle arising from the need to maintain the steam–methane ratio within given bounds to ensure stable combustion of the reformed gas and the necessity to avoid coking in the MSR reactor. The important question at this point is thus to determine the added cost of the CRGT cycle compared with the STIG cycle. A thermoeconomic study of the cycle is therefore necessary to determine the size and catalyst bed volume of the MSR reactor that results in the lowest cost of electricity for the cycle. The methods developed and discussed in this paper are important tools for such a study.

REFERENCES

1 **Olmsted, J. H.** and **Grimes, P. G.** Heat engine efficiency enhancement—through chemical recovery of waste heat. In Proceedings of the Seventh Intersociety Energy Conversion Engineering Conference, 1972, pp. 241–248.

2 **Davidson, B., Dohner, C., Hay, G.** and **Hollenbacher, R.** The intercooled aeroderivative gas turbine—new technology for a rapidly changing electric market. CAGT program progress status report, 1995.

3 **Lloyd, A.** Thermodynamics of chemically recuperated gas turbines. MSc thesis, Center for Energy and Environmental Studies, Princeton University, Princeton, New Jersey, 1991.

4 **Adelman, S. T., Hoffman, M. A.** and **Baughn, J. W.** A methane–steam reformer for a basic chemically recuperated gas turbine. *Trans. ASME, J. Engng for Gas Turbines Power*, 1995, **117**, 16–23.

5 **Janes, J.** Chemically recuperated gas turbine. California Energy Commission Staff Report P500-92-015, 1992.

6 **Rice, I. G.** Split stream boilers for high-temperature/high-pressure topping steam turbine combined cycles. *Trans. ASME, J. Engng for Gas Turbines Power*, 1997, **119**, 385–394.

7 **Botros, K. K., de Boer, M. J.** and **Fletcher, H. G.** Thermodynamic, environmental and economic assessment of CRGT for exhaust heat recovery in remote compressor station applications. In ASME Turbo-Expo '97, Orlando, Florida, 1997, paper 97-GT-510 (American Society of Mechanical Engineers, New York).

8 **Carcasci, C.** and **Facchini, B.** A numerical method for power plant simulations. *Trans. ASME, J. Energy Resources Technol.*, 1996, **118**, 36–43.

9 **Carcasci, C., Facchini, B.** and **Harvey, S.** Modular approach to analysis of chemically recuperated gas turbine cycles. In Proceedings of *Flowers '97*, Florence, Italy, 1997, pp. 1023–1034.

10 **Carcasci, C.** and **Harvey, S.** Design issues for the methane–steam reformer of a chemically recuperated gas turbine. In ASME Turbo-Expo '98, Stockholm, Sweden, 1998, paper 98-GT-35 (American Society of Mechanical Engineers, New York).

11 **Murray, A. P.** and **Snyder, T. S.** Steam–methane reformer kinetic computer model with heat transfer and geometry options. *Ind. Engng Chem., Process Des. Dev.*, 1985, **24**(2), 286–294.

12 **Numaguchi, T.** and **Kikuchi, K.** Intrinsic kinetics and design simulation in a complex reaction network; steam-methane reforming. *Chem. Engng Sci.*, 1988, **43**(8), 2295–2301.

13 **Li, C.** and **Finlayson, B. A.** Heat transfer in packed beds—a revaluation. *Chem. Engng Sci.*, 1977, **32**, 1055–1066.

14 **Ergun, S.** Fluid flow through packed columns. *Chem. Engng Prog.*, 1952, **48**(2), 89–94.

15 **Vampola, J.** Generalization of the laws governing heat transfer and pressure drop during transverse flow gases in finned tube banks. *Heat Mass Transfer*, 1965, **1**, 295–305.

16 *GTPRO: Interactive Software for Gas Turbine Power and Cogeneration System Design*, 1991 (Thermoflow, Sudbury, Massachusetts).

17 **Smith, S. S.** GE aeroderivative gas turbine performance. Report GER-3572B, General Electric Turbine Reference Library, General Electric Power Generation, 1991.

18 *LM2500 Gas Turbine*, Catalogue AE-3232 (12/92), 1992 (General Electric Marine and Industrial Engines).

19 **Carcasci, C., Facchini, B.** and **Harvey, S.** Design and off-design analysis of a CRGT cycle based on the LM2500-STIG gas turbine. In ASME Turbo-Expo '98, Stockholm, Sweden, 1998, paper 98-GT-36 (American Society of Mechanical Engineers, New York).